

# A Linear Programming Relaxation for Binary Tomography with Smoothness Priors

S. Weber<sup>a,\*</sup> C. Schnörr<sup>a</sup> J. Hornegger<sup>b</sup>

<sup>a</sup> *University of Mannheim, Dept. Math. and Comp. Science, CVGPR-Group,  
D-68131 Mannheim, Germany*

*{wstefan, schnoerr}@uni-mannheim.de, www.cvgpr.uni-mannheim.de*

<sup>b</sup> *Siemens Medical Solutions Inc., 91301 Forchheim, Germany  
joachim.hornegger@siemens.com, www.cvgpr.uni-mannheim.de/hornegger*

---

## Abstract

We focus on the reconstruction of binary functions from a small number of X-ray projections. The linear-programming (LP) relaxation to this combinatorial optimization problem due to *Fishburn et al.* is extended to objective functionals with quadratic smoothness priors. We show that the regularized LP-relaxation provides a good approximation and thus allows to bias the reconstruction towards solutions with spatially coherent regions. These solutions can be computed with any interior-point solver and a related rounding technique. Our approach provides an alternative to computationally expensive MCMC-sampling (Markov Chain Monte Carlo) techniques and other heuristic rounding schemes.

*Key words:* Discrete Tomography, Markov Random Fields, Combinatorial Optimization, LP-Relaxation, Approximation Algorithm, Regularization

---

## 1 Introduction

We study the reconstruction of binary functions from a limited number of X-ray projections. The range of angles over which projection rays may vary is limited to the interval  $[0, \pi/2]$ . Therefore the problem falls into the research area of *Discrete Tomography* [1] which generally addresses the problem of reconstructing functions from projection data under imaging conditions where established approaches [2] are not applicable. It is well known that for more

---

\* Corresponding author.

than two projection directions, the reconstruction problem of discrete tomography is NP-hard [3]. Nevertheless, a range of potential applications motivate to investigate polynomial-time algorithms which compute acceptable solutions for related real-world problems.

An interesting LP-relaxation approach to the combinatorial reconstruction problem of discrete tomography was presented in [4]. Assuming feasibility of the original problem, solutions to the relaxed convex optimization problem – which can be computed in polynomial time with interior-point methods – provide useful information about invariant points, i.e. points contained in any solution. A numerical comparison [5] of this approach with ART-like reconstruction [6] and greedy combinatorial optimization [7] yielded promising results. Yet, depending on how severely the reconstruction problem is underdetermined, further constraints and regularization are needed to obtain solutions of higher quality.

A common approach to regularization is to impose priors on the space of solutions. In the discrete case, this leads to a Markov Random Field (MRF) model in terms of a Gibbs distribution by summing up clique potentials over local pixel configurations [8,9]. In the context of discrete tomography, works following this research direction include [10–12]. These approaches differ from each other by the way a local minimum of the objective function is determined: Computationally intensive MCMC-sampling schemes for computing expectations of the posterior distribution [10], filtered backprojection combined with Bayesian restoration [11], or ICM-like local iterative updates in a hierarchical framework [12].

Our approach aims at a direct generalization of the LP-relaxation developed in [4] from binary linear objective functions to binary *quadratic* objective functions which may include Gibbs potentials. To this end, we apply recent results on combinatorial approximation algorithms in the context of MRF-based modeling and optimization [13]. Just as the approach [4], the resulting relaxed optimization problem is convex and the global minimum can straightforwardly be computed by using any interior-point solver. A related scheme for rounding this solution to a binary reconstruction is presented. Thus our approach avoids computationally expensive sampling methods as well as rounding techniques [12,14] which are less understood from the algorithmic point of view (choice of thresholds, convergence).

The paper is organized as follows. In Section 2, we formally state the reconstruction and optimization problem, respectively, and discuss the assumptions involved. The corresponding LP-relaxation is developed next in Section 3. Numerical results are presented and discussed in Section 4. They show that the extended LP-relaxation provides a good approximation and thus improves the reconstruction of spatially coherent functions.

## 2 Problem statement and Approach

Let  $f : \Omega \subset \mathbb{R}^2 \rightarrow \mathbb{R}, y \mapsto f(y)$  be an unknown attenuation function. In order to state the reconstruction problem with respect to  $f$ , we use a discretization model similar to the one in [6] (see Figure 1). The function  $f$  is represented by its values  $x_j \in \{0, 1\}, j = 1, 2, \dots, n, x := (x_1, x_2, \dots, x_n)^T$ , within square pixels. We define  $f(y) := \sum_{j=1}^n x_j \Phi_j(y) = \langle x, \Phi(y) \rangle, \Phi(y) := (\Phi_1(y), \Phi_2(y), \dots, \Phi_n(y))^T$ , where  $\Phi_j(y)$  is 1 if and only if  $y$  lies within the area of the  $j$ th pixel and 0 elsewhere. A number of projection rays  $i = 1, 2, \dots, m$  intersect  $\Omega$ , and the contribution  $A_{ij}$  of each pixel  $j$  is assembled into a  $m \times n$  projection matrix  $A$ . The total attenuation along the  $i$ th ray is represented by the  $i$ th component  $b_i$  of a vector  $b$ .

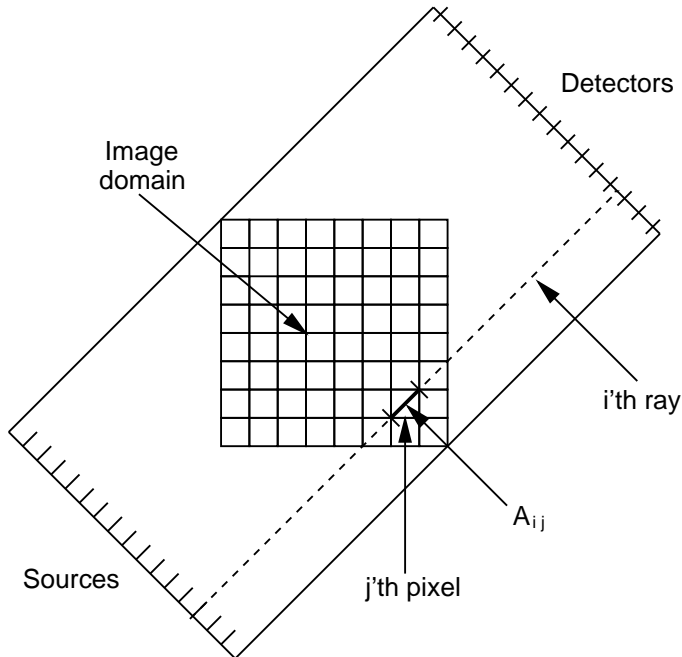


Fig. 1. Discretized model for the discrete tomography reconstruction problem [6].

The imaging process illustrated in Figure 1 thus results in the linear system of equations

$$Ax = b. \quad (1)$$

We note that in order to study separately the extension to *quadratic* objective functionals and corresponding LP-relaxations, we deliberately disregard in this paper any “noise” of the imaging process by assuming  $x_j \in \{0, 1\}, \forall j$ , e.g. ideal projection rays, point sources and detectors.

Fishburn, Schwander, Shepp and Vanderbei [4] proposed the LP-relaxation:

$$(FSSV) \quad \min_{x \in \mathbb{R}^n} 0^\top x, \quad Ax = b, \quad 0 \leq x_j \leq 1, \quad \forall j$$

in order to reconstruct  $x$  by computing a feasible solution to  $(FSSV)$ .

As an alternative, the *Best Inner Fit* criterion for the reconstruction of  $x$  from the projection equations (1) was suggested in [7]. Relaxing the integer constraints  $x_j \in \{0, 1\}, \forall j$ , this leads to the LP-relaxation:

$$(BIF) \quad \max_{x \in \mathbb{R}^n} e^\top x, \quad Ax \leq b, \quad 0 \leq x_j \leq 1, \quad \forall j$$

where  $e^\top = (1, 1, \dots, 1)$ .



Fig. 2. Original ellipses image ( $64 \times 64$ ).

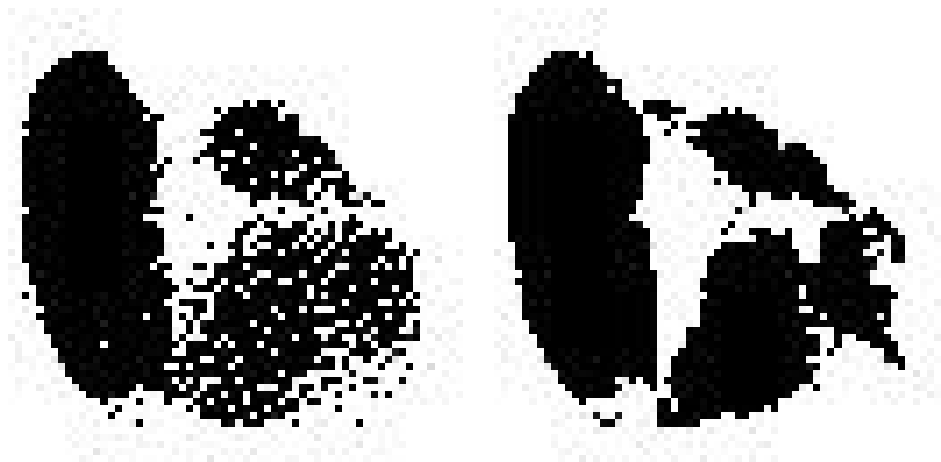


Fig. 3.  $(FSSV)$  (left) and  $(BIF)$  (right) reconstruction from three projections (0, 45, and 90 degree) of ellipses image (figure 2).

Figure 3 illustrates the reconstruction results based on the criteria  $(FSSV)$  and  $(BIF)$ . For both reconstructions three projections were taken from 0, 45, and 90 degree.  $(FSSV)$  yields a solution that fulfills the projection constraints but the reconstructed ellipses are not as coherent anymore as the ones we see in the original image (figure 2). From this point of view  $(BIF)$  achieves a much better result but nevertheless the reconstructed ellipses are blurred. It is not

even possible to determine the number of objects contained in the original image.

### 3 Quadratic Smoothness Functional and LP–Relaxation

The reconstructions shown in the previous section for both the (*FSSV*) and (*BIF*) criterion motivates to consider contextual constraints in order to favor solutions which are spatially more coherent.

A natural way to derive corresponding terms to be added to the the objective functionals (*FSSV*) and (*BIF*) is to consider proper discretizations of smoothness functionals.

$$\|L(f)\|_{L_2}^2, \quad (2)$$

where the operator  $L$  measures the spatial variation of the attenuation function  $x$ . The simplest example for a suitable  $L$  is

$$L(f) = \nabla f = \left( \frac{\partial}{\partial y_1} f, \frac{\partial}{\partial y_2} f \right)^\top \quad (3)$$

Other possible choices include, for instance, the use of a matrix  $W$  depending on the spatial variable  $y$ ,

$$L(f) = W(y) \cdot \nabla f, \quad (4)$$

which leads to a linear anisotropic diffusion process, or the Laplacian

$$L(f) = \Delta f, \quad (5)$$

which results in the biharmonic operator in the corresponding Euler equation.

In this paper, we confine ourselves to the simplest choice (3) which, by discretizing (2), leads to the well-known 5-point stencil for the Laplacian. At the functional level (2), this simply corresponds to summing up the differences at adjacent pixel positions, in our case the 4-neighborhood of a pixel:

$$\sum_{\langle j,k \rangle} (x_j - x_k)^2, \quad (6)$$

where only horizontal and vertical (not diagonal) positions are considered as nearest neighbors.

In order to derive a suitable LP–relaxation based on [13], we replace the squared terms in (6) by their absolute values,

$$\sum_{\langle j,k \rangle} |x_j - x_k|,$$

which in view of the original integer constraint  $x_j \in \{0, 1\}$  is a reasonable approximation, and propose to supplement the objective function (*FSSV*) as follows:

$$(FSSV2) \quad \min_{x \in \mathbb{R}^n} 0^\top x + \frac{\alpha}{2} \sum_{\langle j,k \rangle} |x_j - x_k|, \quad Ax = b$$

Concerning the objective function (*BIF*) we proceed analogously. In addition, we replace the vector  $e$  in the linear term by a weight vector  $c$  indicating the “importance” of each value  $x_j$  with respect to the given data  $b$ :

$$c_j := \prod_i \frac{b_i}{|\Omega \cap \text{ray}(i)|},$$

where  $i$  runs through all projection rays to which  $x_j$  possibly contributes (i.e.,  $A_{ij} \neq 0$ ). This gives:

$$(BIF2) \quad \min_{x \in \mathbb{R}^n} -c^\top x + \frac{\alpha}{2} \sum_{\langle j,k \rangle} |x_j - x_k|, \quad Ax \leq b$$

Following the general approach described in [13], we introduce a vector  $z$  with auxiliary variables  $z^\top = (\dots, z_{\langle j,k \rangle}, \dots)$ , and propose the following LP-relaxations corresponding to (*FSSV2*):

$$(LP1) \quad \begin{aligned} \min_{x,z} 0^\top x + \frac{\alpha}{2} \sum_{\langle j,k \rangle} z_{\langle j,k \rangle} \\ Ax = b \\ z_{\langle j,k \rangle} \geq x_j - x_k \\ z_{\langle j,k \rangle} \geq x_k - x_j \\ 0 \leq x_j \leq 1, \quad \forall j \end{aligned}$$

and (*BIF2*):

$$(LP2) \quad \begin{aligned} \min_{x,z} -c^\top x + \frac{\alpha}{2} \sum_{\langle j,k \rangle} z_{\langle j,k \rangle} \\ Ax \leq b \\ z_{\langle j,k \rangle} \geq x_j - x_k \\ z_{\langle j,k \rangle} \geq x_k - x_j \\ 0 \leq x_j \leq 1, \quad \forall j \end{aligned}$$

## 4 Experimental Evaluation

For our evaluation two different images were used which can be seen in figure 4). The first image ( $64 \times 64$ ) shows three ellipses of different size and orientation

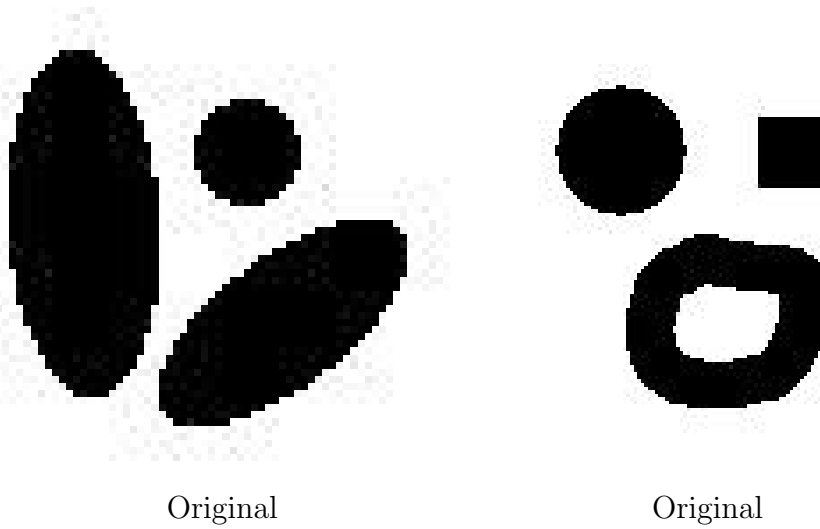


Fig. 4. Original images used for evaluation purposes. On the left side the ellipses image ( $64 \times 64$ ) and on the right side a larger evaluation image ( $128 \times 128$ ).

while the second one ( $128 \times 128$ ) contains a box, a circle, and a donut. For each evaluation we used three projections from 0, 45, and 90 degree according to the discretization scheme illustrated in figure 1. The parameter  $\alpha$  was set to 1.0 throughout all experiments due to empirical reasons.

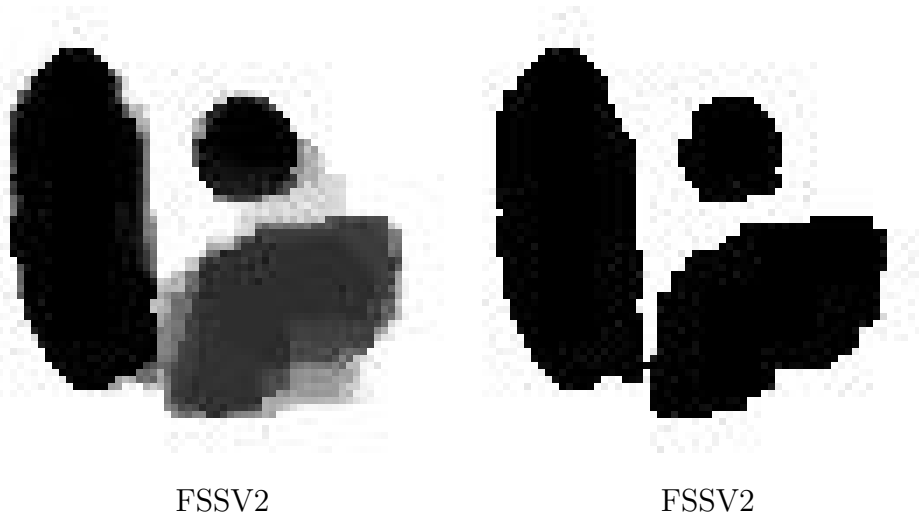


Fig. 5. The left greyvalue image gives the fractional solution output by the LP Solver while the right image shows the binary solution obtained by thresholding (0.5).

Solving the problem with either the (*BIF*), (*FSSV*), (*BIF2*), or (*FSSV2*) method yields a fractional solution in the interval  $[0, 1]$ . In order to obtain a binary solution we applied a threshold at 0.5 to the fractional solution. Kleinberg and Tardos [13] give a randomized rounding technique in order to get binary values for their uniform labeling problem. In our case, however, this method did not achieve better results than a simple threshold. According to the histograms shown in the figures 7, 11, and 12 this is because most of the

$x_j$  are already either 0, 1, or close to one of them.

In Section 2 we have already seen the result of (*FSSV*) and (*BIF*) applied to the ellipses image (figure 3). Compare this to the ellipses reconstructed with (*FSSV2*) (figure 5), all objects are coherent and their shape is closer to the original.

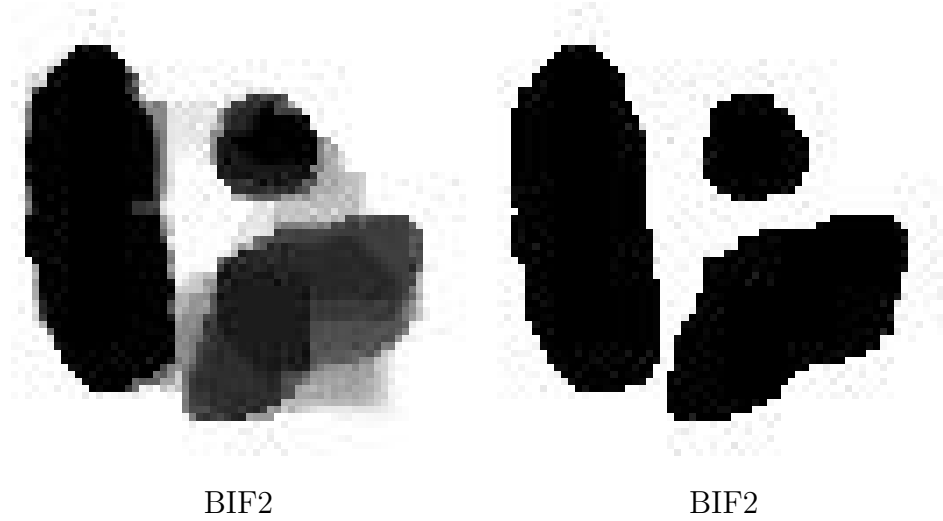


Fig. 6. The left image gives the fractional solution and the right image the binary solution (threshold 0.5).

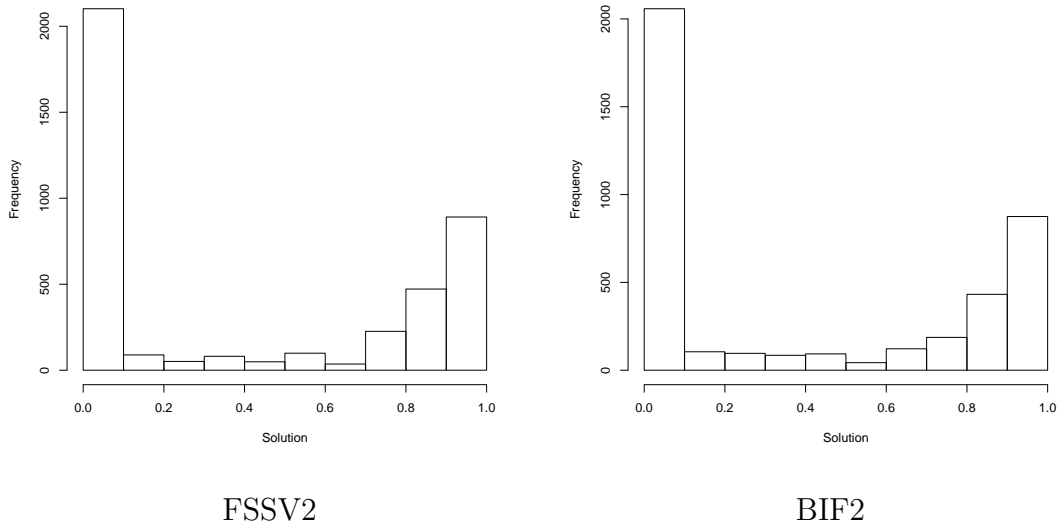


Fig. 7. Histograms of the fractional solutions obtained from the ellipses.

Figure 6 shows the result of the (*BIF2*) reconstruction. All three objects are clearly separated and even smoother than (*FSSV2*) (figure 5).

Figure 8 presents the results achieved by (*FSSV*) and (*BIF*) for the second, slightly more complicated test image. Again we can observe that (*FSSV*) gives an impression of the shape of the original objects but tends to scatter

the pixels in the image domain. The result of ( $BIF$ ) is coherent again but the shape of the objects is blurred.

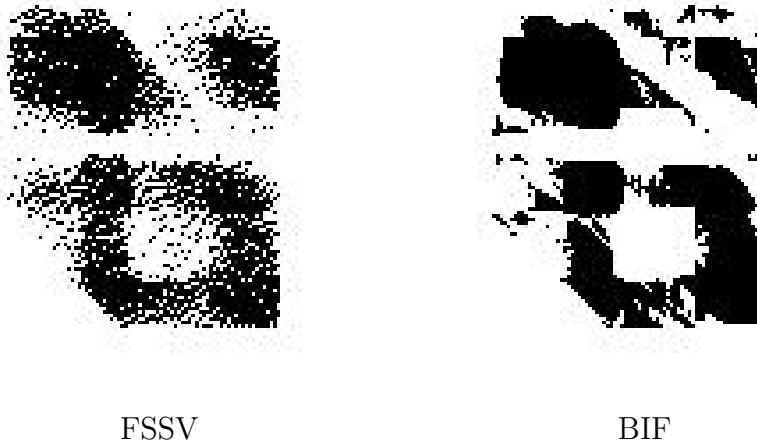


Fig. 8. Reconstruction of the second evaluation image. In case of ( $FSSV$ ) and ( $BIF$ ) we show only the reconstructed binary images and not the fractional solutions because of their similarity.

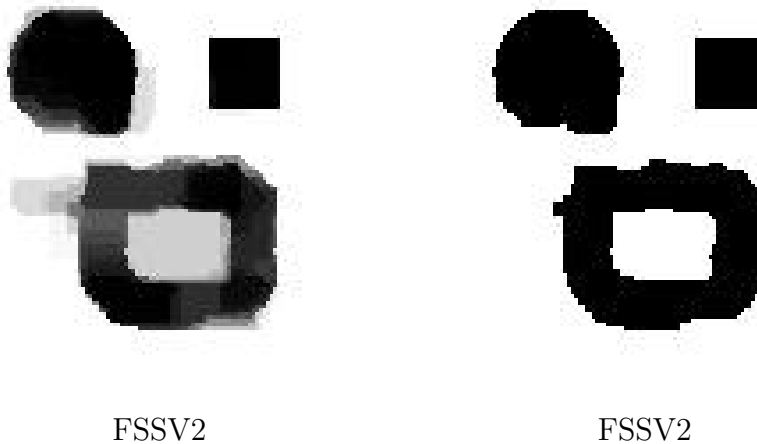


Fig. 9. Reconstruction of the second evaluation image. Left side fractional solution and right side binary solution (threshold 0.5).

The reconstruction of the second image produced by ( $FSSV2$ ) is given in figure 9. All objects can clearly be distinguished and the shape is again very close to the original one. Compared to ( $BIF2$ ) (see figure 10), we can see that both methods accomplished good results. Some object edges are smoother with ( $FSSV2$ ), others are better with ( $BIF2$ ).

For evaluation purposes we used the barrier optimizer that comes with the CPLEX Solver Version 7.5 (<http://www.ilog.com>). The computing time for the ( $FSSV$ ) or ( $BIF$ ) reconstruction of the ellipses image was less than a

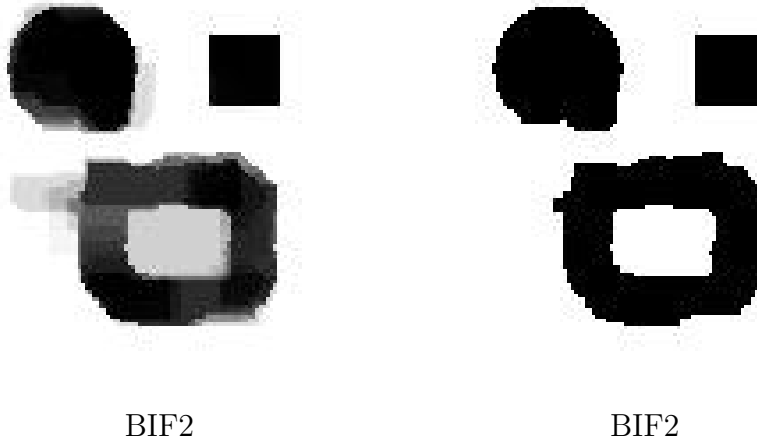


Fig. 10. Reconstruction of the second evaluation image. Left side fractional solution and right side binary solution (threshold 0.5).

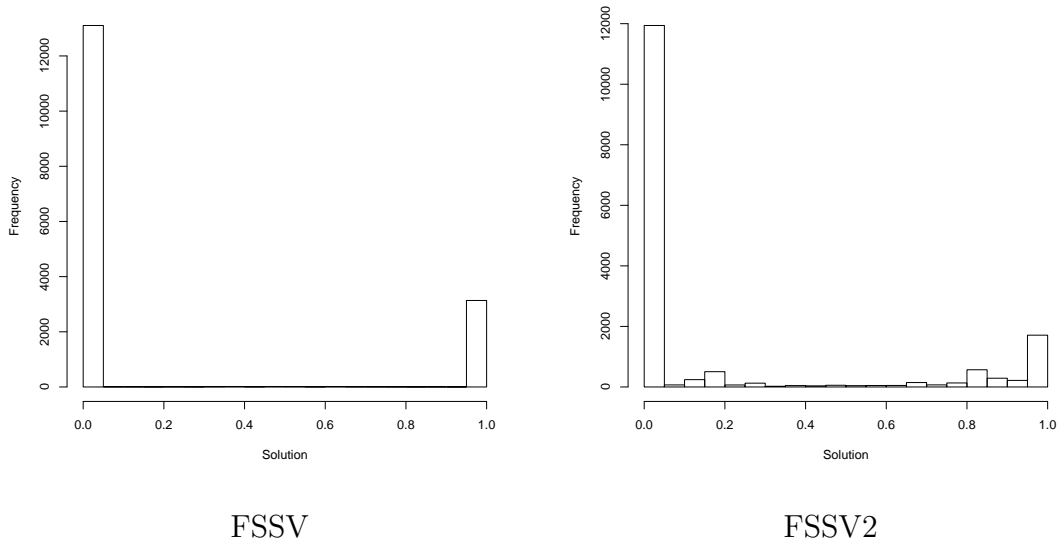


Fig. 11. Histograms of the second evaluation image.

second. The extended versions (*FSSV2*) and (*BIF2*) took about 15 seconds for the ellipses and up to 50 seconds for the larger test image on a 1.2 GHz AMD Athlon.

## 5 Conclusion and Further Work

In this paper we have shown that in case of coherent objects the (*FSSV*) and the (*BIF*) methods can be further improved by introducing additional

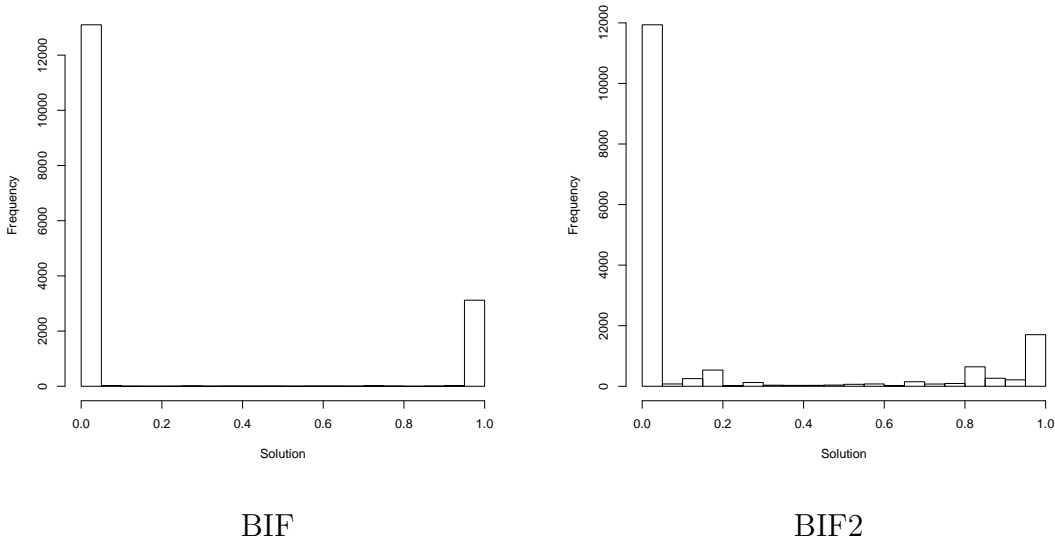


Fig. 12. Histograms of the second evaluation image.

constraints taking the local context into account. This is of particular interest when there are only a limited number of projections available for the reconstruction process. Comparing (*BIF*) to (*FSSV*) we observed that (*BIF*) achieved always a more coherent solution for the problem, whereas the solution of (*FSSV*) gives a better impression of the original shape. We considered only a 4-neighborhood for each pixel, other constellations might be applicable as well. Further we are already working on an adaption to the three dimensional case in which we are particularly interested in due to our medical application background.

## References

- [1] G. Herman and A. Kuba, editors. *Discrete Tomography: Foundations, Algorithms, and Applications*. Birkhäuser Boston, 1999.
- [2] F. Natterer and F. Wübbeling. *Mathematical Methods in Image Reconstruction*. SIAM, Philadelphia, 2001.
- [3] P. Gritzmann, D. Prangenberg, S. de Vries, and M. Wiegelmann. Success and failure of certain reconstruction and uniqueness algorithms in discrete tomography. *Int. J. Imag. Syst. Technol.*, 9:101–109, 1998.
- [4] P. Fishburn, P. Schwander, L. Shepp, and R. Vanderbei. The discrete radon transform and its approximate inversion via linear programming. *Discr. Appl. Math.*, 75:39–61, 1997.
- [5] T. Beck. 3D-Reconstruction of geometrically limited objects with discrete tomography. Master’s thesis, Friedrich-Alexander-Universität Erlangen-

Nürnberg, Lehrstuhl für Künstliche Intelligenz, Inst. für Mathem. Maschinen und Datenverarbeitung, 2002, (in German).

- [6] Y. Censor, D. Gordon, and R. Gordon. Component averaging: An efficient iterative parallel algorithm for large and sparse unstructured problems. *Parallel Computing*, 27:777–808, 2001.
- [7] P. Gritzmann, S. de Vries, and M. Wiegmann. Approximating binary images from discrete X-rays. *SIAM J. Optimization*, 11(2):522–546, 2000.
- [8] S. Geman and D. Geman. Stochastic relaxation, Gibbs distributions, and the Bayesian restoration of images. *IEEE Trans. Patt. Anal. Mach. Intell.*, 6(6):721–741, 1984.
- [9] G. Winkler. *Image Analysis, Random Fields and Dynamic Monte Carlo Methods*, volume 27 of *Appl. of Mathematics*. Springer-Verlag, Heidelberg, 1995.
- [10] S. Matej, G.T. Herman, and A. Vardi. Binary tomography on the hexagonal grid using Gibbs priors. *Int. J. Imag. Syst. Technol.*, 9:126–131, 1998.
- [11] M.T. Chan, G.T. Herman, and E. Levitan. Bayesian image reconstruction using image-modeling Gibbs priors. *Int. J. Imag. Syst. Technol.*, 9:85–98, 1998.
- [12] T. Frese, C.A. Bouman, and K. Sauer. Multiscale Bayesian methods for discrete tomography. In G.T. Herman and A. Kuba, editors, *Discrete Tomography*, pages 237–264. Birkhäuser, 1999.
- [13] J.M. Kleinberg and E. Tardos. Approximation algorithms for classification problems with pairwise relationships: Metric labeling and Markov random fields. In *IEEE Symp. Foundations of Comp. Science*, pages 14–23, 1999.
- [14] Y. Censor. Binary steering in discrete tomography reconstruction with sequential and simultaneous iterative algorithms. *Lin. Algebra and its Appl.*, 339:111–124, 2001.